

# Initial results of imaging melanoma metastasis in resected human lymph nodes using photoacoustic computed tomography

Jithin Jose<sup>1</sup>, Diederik J. Grootendorst<sup>1</sup>, Thomas W. Vijn<sup>1</sup>, Michel Wouters<sup>2</sup>, Hester van Boven<sup>3</sup>, Ton G. van Leeuwen<sup>1,4</sup>, Wiendelt Steenbergen<sup>1</sup>, Theo J.M. Ruers<sup>2,5†</sup> and Srirang Manohar<sup>1\*</sup>

<sup>1</sup>*Biomedical Photonic Imaging Group, MIRA - Institute for Biomedical Technology and Technical Medicine, University of Twente, P.O. Box 217, 7500 AE Enschede, The Netherlands*

<sup>2</sup>*Department of Surgical Oncology, Netherlands Cancer Institute—Antoni van Leeuwenhoek Hospital (NKI-AVL), P.O. Box 90203, 1006 BE Amsterdam, The Netherlands*

<sup>3</sup>*Department of Pathology, Netherlands Cancer Institute—Antoni van Leeuwenhoek Hospital (NKI-AVL), P.O. Box 90203, 1006 BE Amsterdam, The Netherlands*

<sup>4</sup>*Biomedical Engineering and Physics, University of Amsterdam, Academic Medical Center, P.O. Box 22700, 1100 DE, Amsterdam, The Netherlands*

<sup>5</sup>*MIRA - Institute for Biomedical Technology and Technical Medicine, University of Twente, P.O. Box 217, 7500 AE Enschede, The Netherlands*

*\*S.Manohar@utwente.nl, †T. Ruers@nki.nl*

## **Abstract:**

The pathological status of the sentinel lymph node is important for accurate melanoma staging, ascertaining prognosis and planning treatment. The standard procedure involves biopsy of the node and histopathological assessment of its status. Drawbacks of this examination include a finite sampling of the node with the likelihood of missing metastases,

and a significant time-lag before histopathological results are available to the surgeon. We studied the applicability of photoacoustic computed tomographic imaging as an intra-operative modality for examining the status of resected human sentinel lymph nodes. We first applied the technique to image ex vivo pig lymph nodes carrying metastases-simulating melanoma cells using multiple wavelengths. The experience gained was applied to image a suspect human lymph node. We validated the photoacoustic imaging results by comparing a reconstructed slice with a histopathological section through the node. Our results suggest that photoacoustics has the potential to develop into an intra-operative imaging method to detect melanoma metastases in sentinel lymph nodes.

The incidence of cutaneous melanoma, the deadliest form of skin cancer, is a major public health problem around the world. In the United States alone, around 68,000 new cases of skin melanoma were expected in 2010 [1]. In Europe, the estimated figure for 2008 was similar, 67,000 [2]. At the time when incidence of many cancer types is decreasing, melanoma incidence is increasing at the rate of between 3-4% per year. The main reason for this is thought to be increasing intermittent over-exposure to natural ultraviolet light of pale, non-acclimatized caucasian skin.

The treatment for early stage melanoma is primarily focused on wide surgical excision of the primary tumor. For melanomas with an invasion depth (Breslow thickness)  $> 1$  mm, histopathological assessment of the first draining lymph node(s), the sentinel lymph node(s) (SLN), is performed [3]. The pathological status of the SLN is an accurate reflection of the pathological status of the other nodes in the regional nodal basin which in turn is a strong predictor of patient survival [4]. Patients with metastases in their SLNs are treated with radical lymphadenectomy of the other lymph nodes in the regional basin, which has been shown to increase survival [4]. The SLN is identified by lymphatic mapping using

radiocolloid and/or vital blue dye. After excision, the SLN is examined in sections stained with hematoxylin and eosin (H&E), and by immunohistochemical analysis with the use of specific antibodies.

Histopathology in combination with immunohistochemical staining is able to detect micrometastases from clumps right down to solitary melanoma cells. Despite the indisputable merits of the approach, there are disadvantages. The first is related to the act of physically sectioning the structure in finite samples, which leads to an incomplete examination of the node. This could cause micrometastases to be missed leading to false-negative outcomes and wrongly refraining from radical lymphadenectomy. The second disadvantage is that the results of histopathology are not immediately available to the surgeon, taking an average of 4-5 days [5]. In case of tumor positive SLN diagnosis, this implies that complete lymphadenectomy cannot be performed during the sentinel node procedure but has to be planned in a second separate procedure. The two-step surgical procedure: SLN excision and complete lymph node basin excision, is consorted by increased patient discomfort, higher costs, organizational distress and is time-consuming.

These disadvantages could be addressed by the introduction of an intra-operative complete SLN assessment modality, where the excised SLN could be examined in real/near-real time. In the case of a positive SLN a radical lymphadenectomy could be performed directly without scheduling a second surgery at a later date. Methods such as high resolution ultrasound imaging [6] and frozen section histopathological examination [7] have been evaluated as intra-operative techniques to lead to one-step surgery. However these methods have not achieved the required sensitivities, with false negative rates up to 10 % [6].

Photoacoustic (PA) imaging could be one of the technologies able to address these shortcomings. PA imaging is an optical absorption based modality, which uses pulsed laser-induced ultrasound from specific endogenous tissue chromophores (e.g., melanin or

hemoglobin) to map their distribution. In contrast to purely optical imaging, PA imaging retains good spatial resolutions at higher imaging depths since ultrasound waves are not scattered as highly as photons inside biological tissue. Since melanin possesses high optical absorption, melanoma can be detected and imaged using PA imaging without additional labeling.

Viator and co-workers developed PA systems for the *ex vivo* detection of circulating tumor cells (CTC) of melanoma, using piezoelectric detection [8] Zharov *et al* introduced a PA flow cytometry approach for the *in vivo* detection of the presence and concentration of melanoma CTCs in blood [9]. Wang and co-workers obtained *in vivo* three-dimensional (3-D) melanoma images in nude mice using dark-field confocal PA microscopy [10]. More recently, this group went on further to image single melanoma cells *in vivo* using sub-wavelength-resolution PA microscopy [11-12].

The group of Viator advocated the use of PA for detecting melanoma metastases in lymph nodes by using the elevated PA signal responses from melanoma cells implanted in the canine lymph nodes [13], while normal lymph nodes showed low responses. Even though their approach shows high sensitivities, other absorbing structures within nodes also cause PA signals which are difficult to distinguish from melanoma cell responses even when multiple wavelengths are being used. Before PA can be translated to the clinic, an improved method is required which can image the node by mapping various absorbing structures and will allow better discrimination of melanoma cells in the context of known lymph node components/structures such as connective tissue distributions, blood vessels etc.

In this study, we present such an approach using a PA computed tomography (PACT) system, which can generate sliced images of lymph nodes. We show the ability of the system to image micrometastases-simulating melanoma cell clumps in an *ex vivo* animal lymph node. The images are obtained at multiple wavelengths to ascertain wavelength-dependent

contrast of melanoma cells to lymph node tissue. We then present the first imaging findings of a resected human lymph node and compare these with conventional histopathology.

Figure 1 shows the schematic of the top-illumination PACT system. The lymph node is accommodated in a 20 mm deep hollow scooped out from the top of an agar gel cylinder (3% agar, Sigma-Aldrich). The lymph node is immersed in PBS (phosphate buffered saline) inside the hollow, and the agar gel cylinder is mounted in the imaging tank filled with water (Figure 1(b)). Light from an optical parametric oscillator (Opotek, 700-950 nm) pumped by a Q-switched Nd:YAG laser (Brilliant B, Quantel) operating at 10 Hz repetition rate is used to illuminate the node from above. The imager uses a 32-element curvilinear ultrasound detector array (Imasonic, Besançon) with a 32-channel pulser-receiver system (Lecoeur Electronique, Paris) for data acquisition [14]. The piezocomposite elements of the detector have a central frequency of 6.25 MHz with a receiving bandwidth greater than 80%. Each element is shaped to produce an elevation plane focus of 1 mm at a distance of 48 mm from the detector surface. In each channel of the pulser-receiver system the PA signal is amplified by 60 dB, digitized with a sampling rate of 80 MS/s and transferred to the PC. Filtered acoustic backprojection [14] is used to reconstruct the PA images off-line. Prior to each set of measurements, a calibration measurement is performed using a horsetail hair, to ascertain the CT imaging geometry such as centre of rotation, position of detector elements and also the speed of sound in water.

To assess the sensitivity of the system in detecting melanoma cells, we imaged pork lymph nodes, specially prepared to simulate melanoma positive nodes. We first prepared 2% agar solutions in PBS mixed with specific counts of B16 mouse melanoma cells; constant stirring under 30<sup>0</sup> C heating promoted dissolution of agar and homogeneous distribution of the cells. Slowly pipetting out 10  $\mu$ l of the warm mixture using a micropipette with a 20  $\mu$ l tip, resulted in 1-1.5 mm diameter drops which turned into solid beads once they cooled

down. Such agar gel beads embedded with melanoma cells, simulating metastatic clumps, were inserted into a pork lymph node obtained from a butcher. Beads were embedded into the node using a 16G needle. After bead insertion the needle channel is gently squeezed and kneaded closed. Figure 2(a) is the photograph of a pig lymph node with next to it two beads of 10  $\mu$ l volume (roughly 1.5 mm in diameter) containing  $5 \times 10^5$  and  $5 \times 10^4$  melanoma cells. The beads were imaged using 720, 760, 800 and 850 nm with a fluence of  $12 \text{mJcm}^{-2}$  per pulse. Data acquisition per slice for 100 signal averages and 9 projections takes 120 seconds; image reconstruction for a 300x300 pixel image takes 40 seconds. Figure 2(b) is a PA slice image through the center of the node before bead insertion at 6 mm from the top surface. The corresponding PA slice images after the beads were inserted in the lymph node and sealed, are shown in Figs. 2(d)-(e) at wavelengths 720 and 800 nm respectively. The images were acquired at the same height through the node center; Fig.2(c) is a photograph of the cross-section of the lymph node at roughly the same height, exposed using a scalpel. The dotted circles respectively mark the positions of the beads containing  $5 \times 10^5$  and  $5 \times 10^4$  melanoma cells.

The bead with  $5 \times 10^5$  melanoma cells is well depicted in Figs. 2(d) and (e), while the bead with  $5 \times 10^4$  melanoma cells is not visible. The fibrous capsule of the lymph node consisting of trabeculae could be discernable due to collagen, but increased intensity could also be caused by the presence of remnant blood in the blood vessels. Patterns in the lymph node whether with or without the beads (Figs.2(b) (d) and (e)), can also be distinguished, which are most likely collagen associated with the inner trabeculae, which mark the division of the node into follicles. Another source of signal could be blood vessels in the trabeculae. We performed spectral analysis of pixel clusters (10x10 pixel) in melanoma cell regions and the lymph node background regions (border region between 3 and 5 'O' clock in Fig. 2(d)). Figure 2 (f) shows the normalized mean pixel intensity (MPI) against wavelength for the

melanoma bead region and background. Increasing MPI values with decreasing wavelengths are indicative of increased absorption of light by melanin [15].

The imaging of human lymph nodes was based on a study protocol approved by the Medical Ethics Committee (METC) of the Netherlands Cancer Institute—Antoni van Leeuwenhoek Hospital, Amsterdam (NKI-AvL). Patients with the diagnosis of cutaneous melanoma undergoing radical lymphadenectomy following discovery of tumor-positive SLN or clinically detectable nodal recurrence are included in the study after informed consent. Visually identified macroscopic pathological nodes are transported in PBS to the University of Twente, Enschede. After imaging, the nodes are placed in 4% formaldehyde and returned to the Department of Pathology at the NKI-AvL, for standard histopathological examination. Considerations of Good Clinical Practice (GCP) such as maintaining patient anonymity are stringently adhered to. Images using PACT are later correlated with histopathological findings.

A lymph node was obtained from the second echelon lymph node basin from a patient, after regional lymphadenectomy. Figure 3 (a) is a photograph of the node. Eighteen projections of PA signals were obtained in a slice roughly at the center of the node using the same set of wavelengths as before, with a fluence of  $12 \text{ mJcm}^{-2}$  per pulse. Signals were averaged 100 times and each measurement lasted 4 minutes. Figure 3 (b) shows the reconstructed slice at 720 nm approximately 5 mm beneath the nodal surface. The slice shows a diffuse distribution of increased intensity throughout the nodal area. In some regions (between 1 and 4 'o' clock) absorption hot spots are also observed. Figure 3(c) is the gross histopathology section of the lymph node at a depth of 5 mm from the surface.

H&E staining shows that intact melanoma cells are situated throughout the entire node (dark pink) with exception of the center area of the node which is occupied by a necrotic

center (light pink). The size of the histopathological image corresponds with the outline of the photoacoustic image which shows lack of absorption in the right centre of the node corresponding with the location of the necrotic area. In addition, melanoma cell concentrations vary from location to location which could explain the varying contrast throughout the rest of the node. The two images however cannot be compared on a point-by-point basis and show differences in size and locations of the metastasized regions. This could be due to differences in the positions of the slices probed by the two methods. In addition, it is likely that the degree of pigmentation of the metastasized cells in the node is different at different locations: while the PA image will map such a variation, the H&E section does not.

In summary, we showed the first PACT images of melanoma metastasis in a suspect resected human lymph node. The 2-D tomogram of optical absorption showed a gross distribution of melanoma metastases within the node. The histopathological findings supported the images. The human node study protocol was developed based on experiences with phantoms (not shown) and animal lymph nodes. In the latter images, in addition to melanoma cell distributions, we could also recognize absorbing structures reminiscent of trabeculae subdividing the node into follicles. In the animal lymph nodes spectral analysis showed highest contrast at 720 nm.

Further research is required to improve detection capability. In the specific human lymph node studied, melanoma cells dominated the structure, precluding any necessity for the use of spectral analysis. However, situations are expected where absorption from other lymph node constituents are also present in images making melanoma detection challenging. Here a spectral discrimination approach based on the method demonstrated in Fig. 2 (f) will be necessary. Another issue is that image contrast and resolution may not be optimal due to differences in speed-of-sound between the lymph node, water and agar,. In future studies we will apply methods to correct for acoustic velocity [14, 16]. We will also acquire projections

from multiple slices in depth to provide 3-D absorption distributions of the node. This 3-D data set will permit virtual biopsy by visualizing slices in various orientations. The method has potential in future embodiments to develop into a compact intra-operative imaging modality that can be used to assess the resected sentinel lymph nodes.

This research is funded by AgentschapNL through the PRESMITT project IPD067771 in the theme IOP Photonic Devices.

### *References*

1. A. Jemal, R. Siegel, J. Xu, and E. Ward, "Cancer statistics, 2010," *CA Cancer J Clin* **60**, 277-300 (2010).
2. J. Ferlay, D. M. Parkin, and E. Steliarova-Foucher, "Estimates of cancer incidence and mortality in Europe in 2008," *Eur J Cancer* **46**, 765-781 (2010).
3. A. Breslow, "Thickness, cross-sectional areas and depth of invasion in the prognosis of cutaneous melanoma," *Ann Surg* **172**, 902-908 (1970).
4. D. L. Morton, J. F. Thompson, A. J. Cochran, N. Mozzillo, R. Elashoff, R. Essner, O. E. Nieweg, D. F. Roses, H. J. Hoekstra, C. P. Karakousis, D. S. Reintgen, B. J. Coventry, E. C. Glass, and H. J. Wang, "Sentinel-node biopsy or nodal observation in melanoma," *N Engl J Med* **355**, 1307-1317 (2006).
5. D. van der Velde-Zimmermann, M. E. Schipper, R. A. de Weger, A. Hennipman, and I. H. Borel Rinkes, "Sentinel node biopsies in melanoma patients: a protocol for accurate, efficient, and cost-effective analysis by preselection for immunohistochemistry on the basis of Tyr-PCR," *Ann Surg Oncol* **7**, 51-54 (2000).
6. A. Sanki, R. F. Uren, M. Moncrieff, K. L. Tran, R. A. Scolyer, H. Y. Lin, and J. F. Thompson, "Targeted high-resolution ultrasound is not an effective substitute for sentinel lymph node biopsy in patients with primary cutaneous melanoma," *J Clin Oncol* **27**, 5614-5619 (2009).
7. A. Stojadinovic, P. J. Allen, B. M. Clary, K. J. Busam, and D. G. Coit, "Value of frozen-section analysis of sentinel lymph nodes for primary cutaneous malignant melanoma," *Ann Surg* **235**, 92-98 (2002).
8. R. M. Weight, J. A. Viator, P. S. Dale, C. W. Caldwell, and A. E. Lisle, "Photoacoustic detection of metastatic melanoma cells in the human circulatory system," *Opt Lett* **31**, 2998-3000 (2006).
9. V. P. Zharov, E. I. Galanzha, E. V. Shashkov, N. G. Khlebtsov, and V. V. Tuchin, "In vivo photoacoustic flow cytometry for monitoring of circulating single cancer cells and contrast agents," *Opt Lett* **31**, 3623-3625 (2006).
10. J. T. Oh, M. L. Li, H. F. Zhang, K. Maslov, G. Stoica, and L. H. V. Wang, "Three-dimensional imaging of skin melanoma in vivo by dual-wavelength photoacoustic microscopy," *J Biomed Opt* **11**, - (2006).

11. C. Zhang, K. Maslov, and L. V. Wang, "Subwavelength-resolution label-free photoacoustic microscopy of optical absorption in vivo," *Opt Lett* 35, 3195-3197 (2010).
12. T. N. Erpelding, C. Kim, M. Pramanik, L. Jankovic, K. Maslov, Z. Guo, J. A. Margenthaler, M. D. Pashley, and L. V. Wang, "Sentinel lymph nodes in the rat: noninvasive photoacoustic and US imaging with a clinical US system," *Radiology* 256, 102-110 (2010).
13. D. McCormack, M. Al-Shaer, B. S. Goldschmidt, P. S. Dale, C. Henry, C. Papageorgio, K. Bhattacharyya, and J. A. Viator, "Photoacoustic detection of melanoma micrometastasis in sentinel lymph nodes," *J Biomech Eng* 131, 074519 (2009).
14. J. Jose, R. G. H. Willeminck, S. Resink, D. Piras, J. C. G. van Hespén, C. H. Slump, W. Steenbergen, T. G. van Leeuwen, and S. Manohar, "Passive element enriched photoacoustic computed tomography (PER PACT) for simultaneous imaging of acoustic propagation properties and light absorption," *Opt. Express* 19, 2093-2104 (2011).
15. G. Zonios, A. Dimou, I. Bassukas, D. Galaris, A. Tsolakidis, and E. Kaxiras, "Melanin absorption spectroscopy: new method for noninvasive skin investigation and melanoma detection," *J Biomed Opt* 13, 014017 (2008).
16. S. Manohar, R. G. H. Willeminck, F. van der Heijden, C. H. Slump, and T. G. van Leeuwen, "Concomitant speed-of-sound tomography in photoacoustic imaging," *Appl Phys Lett* 91, - (2007).

## FIGURE CAPTIONS

Figure 1: The photoacoustic tomographic (PACT) instrument utilizing top-illumination. The lymph node is placed in PBS in a hollow in the agar gel cylinder. The detector array is rotated around the object in water.

Figure 2: (a) Photograph of the pig lymph node and agar gel beads embedded with melanoma cells, the darker bead carrying  $5 \times 10^5$  cells and the other  $5 \times 10^4$  cells, (b) PACT image using 720 nm light of the node prior to bead-insertion, (c) Photograph of sliced lymph node exposing the beads; the right dotted circle marks the  $5 \times 10^5$  cell bead and left dotted circle marks the  $5 \times 10^4$  cell bead, (d) and (e) are the PACT images of the lymph node after bead-insertion using wavelengths of excitation 720 nm, and 800nm. (f) normalized mean pixel intensity (MPI) of the melanoma bead and the background lymph node plotted against wavelength.

Figure 3: (a) Photograph of the resected human lymph node, (b) Photoacoustic slice image in roughly the center of the node using 720 nm excitation, showing a diffuse speckled distribution of high absorption. The right centre of the node does not contain these high absorption characteristics. (c) histopathology (H&E) section of the corresponding slice; the darker regions correspond with melanoma cells and the lighter region in the right centre is indicative for a necrotic area. (See text for details.)

## FIGURES

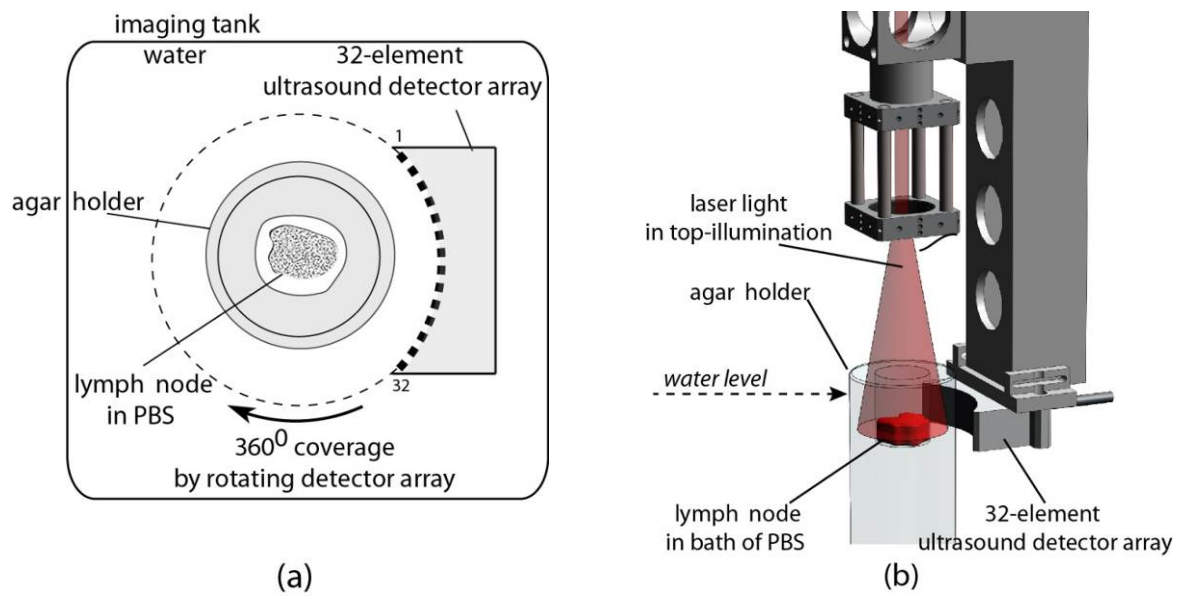


Figure 1: The photoacoustic tomographic (PACT) instrument utilizing top-illumination. The lymph node is placed in PBS in a hollow in the agar gel cylinder. The detector array is rotated around the object in water.

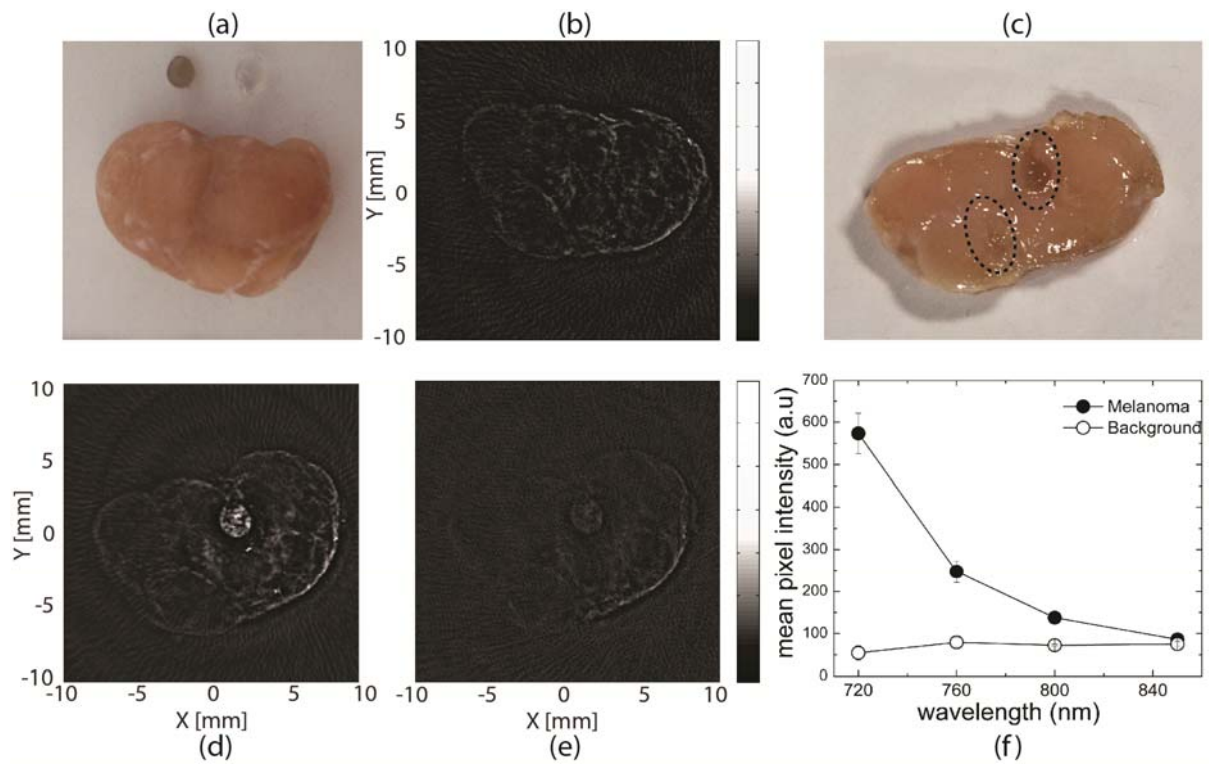


Figure 2: (a) Photograph of the pig lymph node and agar gel beads embedded with melanoma cells, the darker bead carrying  $5 \times 10^5$  cells and the other  $5 \times 10^4$  cells, (b) PACT image using 720 nm light of the node prior to bead-insertion, (c) Photograph of sliced lymph node exposing the beads; the right dotted circle marks the  $5 \times 10^5$  cell bead and left dotted circle marks the  $5 \times 10^4$  cell bead, (d) and (e) are the PACT images of the lymph node after bead-insertion using wavelengths of excitation 720 nm, and 800nm. (f) normalized mean pixel intensity (MPI) of the melanoma bead and the background lymph node plotted against wavelength.

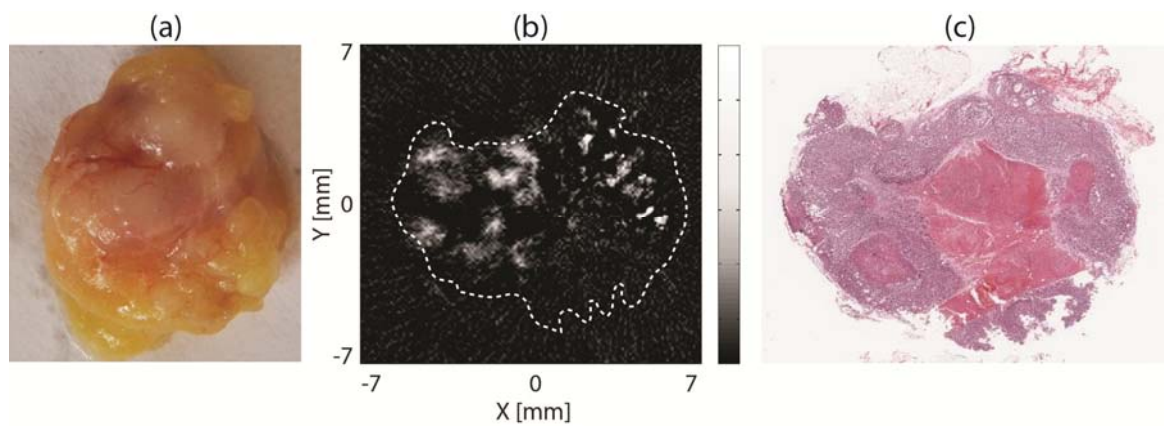


Figure 3: (a) Photograph of the resected human lymph node, (b) Photoacoustic slice image in roughly the center of the node using 720 nm excitation, showing a diffuse speckled distribution of high absorption. The right centre of the node does not contain these high absorption characteristics. (c) histopathology (H&E) section of the corresponding slice; the darker regions correspond with melanoma cells and the lighter region in the right centre is indicative for a necrotic area. (See text for details.)